Control of the RMS Output Current in Series Resonant Converters

Manon Doré, Nicola Zaupa

Control of the RMS Output Current in Series Resonant Converters

Manon Doré * **Nicola Zaupa** *

* *LAAS-CNRS, Université de Toulouse, CNRS, Toulouse, France (e-mail: {mdore,nzaupa}@laas.fr).*

Abstract: In this work the problem of regulation of the Root Mean Square (RMS) value of the current for Series Resonant Converter (SRC) is addressed. The self-oscillating behavior is ensured by an amplitude-modulation like control law and the RMS value is estimated with a proposed hybrid system. The closed-loop regulation is done with a Proportional-Integral (PI) controller with anti-windup scheme, and a set of Linear Matrix Inequalities (LMIs) is introduced to tune the gains. The knowledge of a reference trajectory is not needed to implement the controller, and it is shown to be effective in simulation considering uncertain parameters.

Keywords: Power and Energy Control, Control of Nonlinear Systems, Hybrid Systems, Anti-windup, PI-controller, Resonant Converters.

1. INTRODUCTION

The resonant converter is a power converter topology that takes advantages of the resonance phenomenon in order to reduce losses and achieve high efficiency. It transforms a DC input to a high-frequency AC output; a resonant DC-DC converter can be built by rectifying the output of the resonant tank. It is also characterized by a soft-switching characteristics, reduced switching losses and high power factor, if it operates near the resonant frequency. Those features made it popular for applications in various fields, such as battery chargers (Deng et al., 2014), inductive heating (Lucia et al., 2009), electronic ballast (Yin et al., 2003), and medical application (Cavalcante, 2006).

The resonant tank is composed of an L–C network; it is driven by an H-Bridge, whose output voltage is controlled in order to achieve a desired behavior. Resonant converters are characterized by sinusoidal signals; since the range of variation of these signals is usually large, small signal approximation is not applied but rather first harmonic approximation is used (Erickson and Maksimović, 2020).

This kind of converters are supposed to operate near the resonant frequency in order to reduce the losses since they are designed for a limited bandwidth. To ensure the oscillations, different solutions can be adopted (Youssef and Jain, 2004): frequency modulation, phase-shift modulation, pulse density modulation, zero voltage or current switching, and resonant frequency tracking. Among them, *self-oscillating* resonant converters are characterized by the fact they are able to ensure the oscillation without using an external oscillator or without knowing the resonant frequency (Pinheiro et al., 1999). Several works have been proposed to regulate the SRC, including techniques based on optimal trajectory computation (Oruganti et al., 1987), state plane criteria with reference on the limit-cycle amplitude (Bonache-Samaniego et al., 2017), geometric criteria (Mohammadi and Ordonez, 2016), and adaptation scheme (Sebastián et al., 2022), among many others.

In this work, a closed-loop control scheme is proposed to achieve regulation of the RMS value of the current flowing in the resistive load of an SRC, whose schematic is shown in Fig. 1. In order to achieve that:

a) the self-oscillating behavior is ensured by an inner control loop based on (Zaupa et al., 2023);
b) the RMS value is estimated with a proposed hybrid dynamical system;
c) the output regulation is performed by an outer control loop constituted by a PI controller with anti-windup.

The self-oscillating control law proposed in (Zaupa et al., 2023) ensures that there exist a unique limit cycle, and that the oscillating frequency is almost constant and near the resonant one, for any given control parameter $\varphi \in [0, \pi/2)$. The relation between φ and the output amplitude is characterized more in details. The RMS value estimator is a hybrid systems that does not need any tuning and retrieve a piece-wise constant output at every half-cycle. In Section 2, the converter and the RMS value estimator are described, and then they are approximated as a first order system. This approximation allows designing a linear PI controller that includes an anti-windup scheme. The design process is discussed in Section 3 and a LMI-based formulation – which considers uncertain parameters – is proposed in order to design the gains. In Section 4, the proposed control scheme is validated by simulations, which show the effectiveness and the robustness to uncertainties.

Notation. $\mathbb{R}$ ($\mathbb{R}_{\geq 0}$) is the set of real (nonnegative) numbers. $\mathbb{S}^n$ denotes the set of square positive definite matrices of dimension $n \times n$. To compact the notation, given a square matrix M, we denote $\mathrm{He}(M) := M + M^\top$. The stacking of vectors $u \in \mathbb{R}^n$ and $v \in \mathbb{R}^m$ is denoted in a compact way as $(u, v) := \begin{bmatrix} u^\top & v^\top \end{bmatrix}^\top \in \mathbb{R}^{n+m}$, where $u^\top$ denotes the transpose of u.

⋆ The authors have contributed in equal parts to the work.

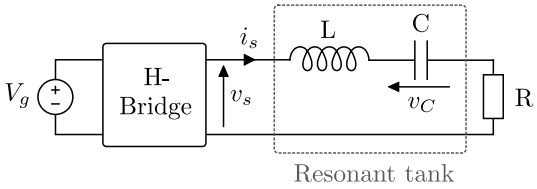

Fig. 1. Circuit of the series resonant converter.

2. MODELING

In this section we are going to discuss the dynamical model of the resonant converter and the hybrid dynamical system to estimate the RMS value.

2.1 Converter dynamics

The SRC schematic is given in Fig. 1. The H-Bridge, fed by a DC input voltage V_g, generates the voltage $v_s = \sigma V_g$ with $\sigma \in \{-1, 0, 1\}$, according to the position of the switches of the H-Bridge. The inductor and the capacitor form the resonant tank, which is driven by the voltage v_s. Inspired by (Zaupa et al., 2023), the system dynamics can be described by the normalized state variables

$$x_1 := \frac{v_C}{V_g}, \quad x_2 := \frac{1}{V_g}\sqrt{\frac{L}{C}} i_s. \tag{1}$$

This allows writing the dynamics of the converter as

$$\dot{x} = f(x, \sigma) := \begin{bmatrix} 0 & \omega_0 \\ -\omega_0 & -\beta \end{bmatrix} x + \begin{bmatrix} 0 \\ \omega_0 \end{bmatrix} \sigma, \tag{2}$$

where $x = (x_1, x_2)$, $\omega_0 := (\sqrt{LC})^{-1}$ is the resonant frequency and $\beta = R/L$ is the internal dissipation. The quality factor is defined as $Q := \omega_0/\beta$ and gives an important information about the waveform of the signals in the converter and the frequency response.

Our objective is to control the RMS value of the output current i_s, which corresponds to control the RMS value of the state x_2 that is proportional to i_s. Therefore, a reference on i_s can be directly cast as a reference on x_2.

As anticipated in the introduction, to further analyze the circuit we consider a first harmonic approximation. This is possible under the following Hypothesis (Erickson and Maksimović, 2020, Ch. 19).

Hypothesis 1. The converter has a high quality factor Q and it works in continuous conduction mode.

Intuitively, this can be translated into the fact that the signals are almost sinusoidal. Otherwise, having a small quality factor implies that the signals are composed of more harmonics since they are not filtered out. This hypothesis is reasonable in most of the operating conditions. For an SRC, this is no more valid as soon as the load increases (i.e. Q decreases). Anyway, variations on the value of Q will be considered in the design of the control loop, so as to make it more robust with respect to the non-modeled effects and perturbations. This will make the converter work also with low Q.

2.2 Inner Oscillation controller

The inner controller takes care of ensuring the self-oscillating behavior. In (Zaupa et al., 2023), an hybrid control law has been proposed to control the output of the H-bridge in a three level fashion. It allows working near the resonance frequency without the need of an external oscillator, and the amplitude modulation behavior is ensured thanks to a control law based on the phase-plane.

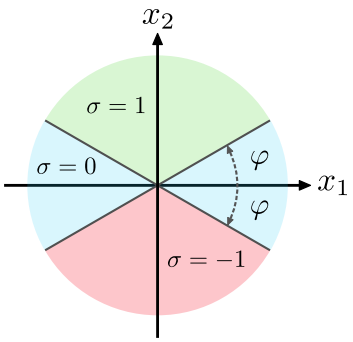

Fig. 2. Representation of the four zones used by the inner control (3) and of the parameter φ.

That control law can be formulated in an equivalent way in the phase-plane (x_1, x_2). Basically, four zones are defined in the phase-plane and, according to the current value of the state, the input σ is retrieved obtained. The zones are depicted in Fig. 2. There are two cones of aperture 2φ in which $\sigma = 0$ (symmetric with respect to the axes); a the upper cone with $\sigma = 1$; and a the lower cone where $\sigma = -1$. Therefore, we can write the following control law

$$\sigma = \begin{cases} 0, & \text{if } x_1^2 \sin^2\varphi - x_2^2 \cos^2\varphi \geq 0, \\ \text{sign}(x_2), & \text{otherwise.} \end{cases} \tag{3}$$

Since this control law is equivalent to the one in (Zaupa et al., 2023), the following result is inherited. For a more comprehensive understanding, we suggest to consult the detailed exposition in (Zaupa et al., 2023).

Proposition 2. Under the condition $Q > 0.5$ (the resonant tank is underdamped), for every $\varphi \in [0, \pi/2)$, the closed-loop (2), (3) has a unique stable and almost globally attractive periodic orbit with basin of attraction $\mathbb{R}^2 \backslash (0, 0)$.

Remark 3. The limit case $\varphi = \pi/2$ corresponds to have $\sigma = 0$ for all the time, therefore the trajectories will converge toward the origin while oscillating due to the underdamped behavior.

The parameter φ induces the desired amplitude modulation behavior since it acts on the harmonics of σ. From (Pitel, 1986), σ can be expressed by the Fourier expansion

$$\sigma = \frac{4}{\pi} \sum_{n=1,3,\cdots}^{\infty} \cos\varphi \frac{\sin\frac{n\pi}{2}}{n} \sin(n\omega t), \tag{4}$$

where we can remark that the amplitude of the first harmonic corresponds to $\frac{4}{\pi}\cos\varphi$, and ω is a generic oscillating frequency. Moreover, assuming that the oscillating frequency is almost constant and near ω_0, we know that the static gain between the first harmonic of σ and the amplitude of x_2 corresponds to the quality factor Q. This let us to conclude, using (4), that an approximated expression between φ and the amplitude of x_2 is

$$x_{2\text{peak}} \simeq \frac{4}{\pi} Q \cos\varphi. \tag{5}$$

2.3 RMS value estimation

As a reminder, the RMS value of a periodic signal $\delta(t)$ is given by

$$\delta_{\text{RMS}} := \sqrt{\frac{1}{T_2 - T_1}\int_{T_1}^{T_2} \delta^2(t)dt},$$

with $T_2 - T_1 > 0$ the period of the signal. In particular, it is well-known that the RMS value of a sinusoidal signal $\bar{\delta}(t) = \Delta \sin(\omega t)$ is $\bar{\delta}_{\text{RMS}} = \frac{|\Delta|}{\sqrt{2}}$.

Since calculating the RMS value involves an integral over the period of the signal, it is challenging to have a continuous measure of it. Additionally, the period should be known. To overcome this, a dynamical system is introduced to estimate the RMS value. To this end, the following hypothesis – realistic in our case – is done.

Hypothesis 4. The signal at the steady state is periodic with zero dc component and different from zero.

It allows simplifying the analysis since we are sure that the signal will pass through zero (i.e. there will be a zero crossing) and that the integral over a half-period is half the integral over one period. Therefore, without loss of generality, we can compute the RMS value by considering the half period. The idea is to introduce a hybrid dynamical system, based on the formalism of (Goebel et al., 2012), that is able to estimate the RMS value of a signal. It consists in an integrator of the squared input signal between two zero crossing, and a timer that measures the elapsed time. These two information let us reconstruct the RMS value as a piece-wise constant function, which is enough for our case.

Simple RMS value estimator The simple and intuitive hybrid dynamical system that we can write is

$$\begin{aligned}(\dot{\xi}, \dot{\eta}, \dot{\Xi}, \dot{T}) &= (\delta^2, 1, 0, 0), \quad \text{if } \delta \neq 0,\\ (\xi^+, \eta^+, \Xi^+, T^+) &= (0, 0, \xi, \eta), \quad \text{if } \delta = 0.\end{aligned} \tag{6}$$

Over a half-period, $\xi \in \mathbb{R}_{\geq 0}$ keeps track of the integral of the square of the signal $\delta(t)$ and $\eta \in \mathbb{R}_{\geq 0}$ counts the elapsed time. At the zero-crossings, the states ξ and η are reset and their previous values are stored in Ξ and T, which are used to calculate the RMS value of δ as $\sqrt{\Xi/T}$. The behavior of the hybrid systems is shown in Fig. 3. We can see that the output is constant and matches the theoretical RMS value once the signal reaches the steady state, the estimation is delayed approximately of half-period.

Robust RMS value estimator Nevertheless, system (6) is not robust with respect to perturbations that are usually present in physical or sampled systems; this implies that a zero-crossing can be missed. To amount for this, since we want to estimate the RMS value of x_2, we can take advantage of the knowledge of the dynamics (2). Inspired by (Goebel et al., 2012, Example 4.18), we introduce the memory variable p, which keeps track of where the zero-crossing happens in the phase-plane (x_1, x_2). We can rewrite (6) as

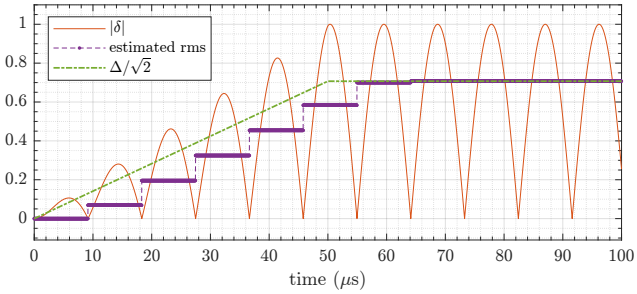

Fig. 3. Behavior of the proposed hybrid systems (6). The input $\delta(t)$ is a sine wave modulated by a ramp. The dashed-dotted line is a reference RMS value (amplitude of the sinus over $\sqrt{2}$) and the solid line is the estimated RMS value estimated by the hybrid systems.

$$\begin{bmatrix}\dot{x}\\ \dot{\xi}\\ \dot{\eta}\\ \dot{\Xi}\\ \dot{T}\\ \dot{p}\end{bmatrix} = \begin{bmatrix}f(x,\sigma)\\ {x_2}^2\\ 1\\ 0\\ 0\\ 0\end{bmatrix}, \qquad \text{if } (x, \xi, \eta, \Xi, T, p) \in C, \tag{7a}$$

$$\begin{bmatrix}x^+\\ \xi^+\\ \eta^+\\ \Xi^+\\ T^+\\ p^+\end{bmatrix} = \begin{bmatrix}x\\ 0\\ 0\\ \xi\\ \eta\\ -\text{sign}(x_1)\end{bmatrix}, \qquad \text{if } (x, \xi, \eta, \Xi, T, p) \in D, \tag{7b}$$

where σ is defined in (3), and the flow set C and jump set D are defined as

$$C := \{(\xi, \eta, \Xi, T, p) \in \mathbb{R}^4_{\geq 0} \times \{-1, 1\} \ : \ px_2 \geq 0\}, \tag{7c}$$

$$D := \{(\xi, \eta, \Xi, T, p) \in \mathbb{R}^4_{\geq 0} \times \{-1, 1\} \ : \ px_2 \leq 0, px_1 \geq 0\}. \tag{7d}$$

Let us notice that the dynamics of x is not affected by the overhead of the RMS value estimator, and that the state x is necessary also for the inner control (3), hence, no extra measurement is required. Then, the RMS value of x_2 can be expressed as

$$y := x_{2\text{RMS}} = \sqrt{\frac{\Xi}{T}}. \tag{7e}$$

What changes with respect to (6) is that the zero-crossing is detected over a surface. Once the jump set is reached, the solution cannot flow anymore and it is forced to jump, which corresponds to a zero-crossing detection.

2.4 First order approximation of the open loop

To analyze the closed-loop system and design the controller in a tractable way, we aim at approximating the expression between y and y_{in} in Fig. 4.

First of all, let us notice that an approximated expression for the relation between φ and the RMS value of x_2, when the signals are almost sinusoidal, is

$$x_{2\text{RMS}} \simeq \frac{x_{2\text{peak}}}{\sqrt{2}} \simeq \frac{4Q}{\pi\sqrt{2}} \cos\varphi =: \gamma \cos\varphi, \tag{8}$$

where γ represents the gain between σ and the RMS value of x_2 for $\varphi = 0$. We can use the inverse of this expression

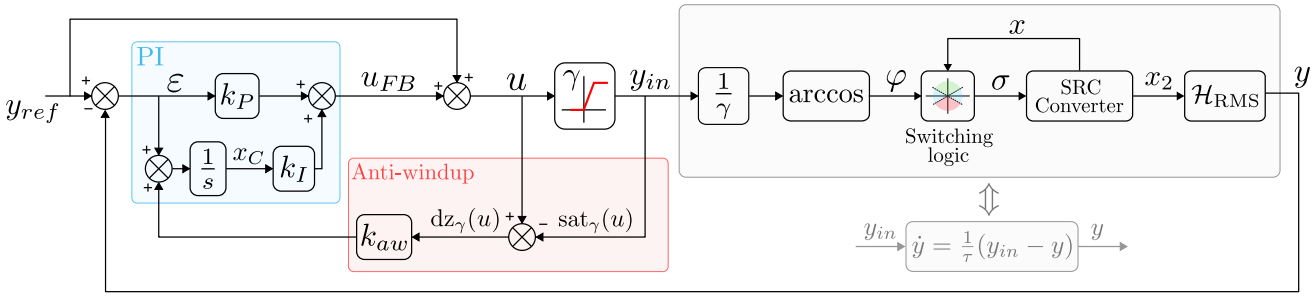

Fig. 4. Control scheme. The controller is on the left (PI and Anti-windup) while the plant, which is approximated to a first-order systems, is on the right.

to find the value of φ in order to obtain the desired RMS value y_{in}

$$\varphi = \arccos\left(\frac{y_{in}}{\gamma}\right). \tag{9}$$

This amounts for the static relation. Essentially, once a reference RMS value y_{in} is given: it is transformed into φ by (9); oscillations are ensured at the proper amplitude by the inner control (3); and the RMS value y is estimated by the hybrid systems (7). For the dynamic part, a first order dynamics is considered between the input y_{in} and the output y with unitary static gain

$$\dot{y} = \frac{1}{\tau}(-y + y_{in}). \tag{10}$$

Since the dominant dynamics is the one of the resonant tank, the time constant τ can be defined as $\tau := \frac{2}{\beta}$. To explain this, let us consider a step input on y_{in}, which is equivalent to a step change in the amplitude of the first harmonic of σ since the relation is algebraic. This step in the amplitude is applied to the dynamics (2). To simplify the expressions, we consider that the converter is oscillating at the resonant frequency ω_0. Considering the analysis of second order linear systems with sinusoidal input, if we apply the input $\sigma = a_0 \sin(\omega_0 t)$ to (2), we have the following response

$$x_2(t) = \underbrace{Q a_0 \sin(\omega_0 t)}_{\text{steady-state}} + \underbrace{a_1 \mathrm{e}^{-\frac{\beta}{2}t} \sin(a_2 t)}_{transient},$$

where a_1 and a_2 are two constants depending on the parameter of the system. Therefore, the output is a sum of two terms: a sinusoidal signal with the same frequency and a gain corresponding to Q as expressed in (5), counting for the steady-state part (frequency analysis results apply); and a transient component composed by a sinus modulated by an exponential function with decay constant $2/\beta$. This decay rate represents the dominant dynamics for the transient behavior of the overall chain. To validate this results, Fig. 5 illustrates the step response of y computed with (7) and y from (10), when a step affect y_{in}. The first order behavior and link between the two system can be clearly observed.

3. OUTPUT REGULATION

The control objective is the regulation of the RMS value of x_2. Since the open-loop is approximated as a first order dynamics, a simple and effective controller that can be implemented is a PI with a feed-forward component. This allows also compensating for inaccuracies in the model and

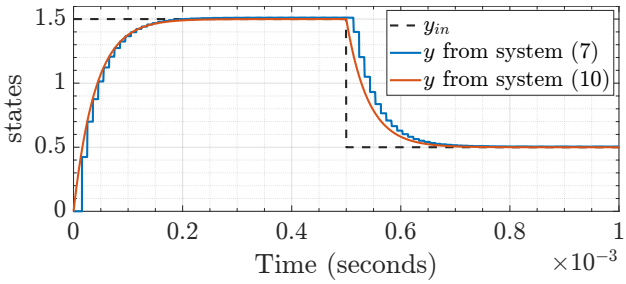

Fig. 5. Step of y_{in} response of y computed with (7) and y from (10).

limited nonlinearities, e.g. the signals are not sinusoidal and the parameters of the converter are not exactly known.

3.1 Closed-loop description

The first order dynamics (10) has a limit in the input values y_{in} that it can take due to the arccosine function. This fact is modeled as a saturation

$$\mathrm{sat}_\gamma(u) = \begin{cases} \gamma, & \text{if } u \geq \gamma, \\ u, & \text{if } 0 \leq u \leq \gamma, \\ 0, & \text{if } u \leq 0, \end{cases}$$

so that the input of the arccosine function is limited in the range $[0, 1]$, which corresponds to φ being in the correct range $[0, \pi/2]$. Having the saturation element to ensure that the control is bounded in the allowed interval, the implementation of an anti-windup scheme follows naturally (Tarbouriech et al., 2011). The aim of the anti-windup is to improve the behavior of the closed-loop when the saturation is active.

The complete scheme of the closed-loop system is given in Fig. 4 and the dynamical equations governing it are

$$\begin{cases} \dot{y} &= \tau^{-1}(-y + u - \mathrm{dz}_\gamma(u)), \\ \dot{x}_c &= y_{ref} - y + k_{aw}\,\mathrm{dz}_\gamma(u), \\ u &= k_P \varepsilon + k_I x_c + y_{ref}, \end{cases} \tag{11}$$

where $\mathrm{dz}_\gamma(u) := u - \mathrm{sat}_\gamma(u)$ is the deadzone function. Thereafter, we rewrite the dynamics in error coordinates considering $\varepsilon := y_{ref} - y$, and $u_{\mathrm{FB}} := u - y_{ref}$. Notice that $\mathrm{dz}_\gamma(u) = \mathrm{dz}(u_{\mathrm{FB}})$, where $\mathrm{dz}(u_{\mathrm{FB}})$ is defined by the saturation function

$$\mathrm{sat}(u_{\mathrm{FB}}) = \begin{cases} \gamma - y_{ref}, & \text{if } u_{\mathrm{FB}} \geq \gamma - y_{ref}, \\ u_{\mathrm{FB}}, & \text{if } -y_{ref} \leq u_{\mathrm{FB}} \leq \gamma - y_{ref}, \\ -y_{ref}, & \text{if } u_{\mathrm{FB}} \leq -y_{ref}. \end{cases}$$

With this change of coordinates, dynamics (11) can be written as

Table 1. System parameters.

Components parameters	Corresponding system characteristics
$V_g = 24$ V	$Q \in [1, 10]$
$R \in [0.316, 3.16]\ \Omega$	$\omega_0 = 3.16 \times 10^5\ rad/s$
$L = 10\ \mu$H	$\beta \in [3.16 \times 10^4, 3.16 \times 10^5]$
$C = 1\ \mu$F	$\tau \in [6.32, 63.25]\ \mu$s

$$\begin{cases} \dot{\varepsilon} &= \tau^{-1}(-\varepsilon - u_{\text{FB}} + \text{dz}(u_{\text{FB}})) \\ \dot{x}_c &= \varepsilon + k_{aw}\,\text{dz}_\gamma(u_{\text{FB}}) \\ u_{\text{FB}} &= k_P\varepsilon + k_I x_c \end{cases} \tag{12}$$

To simplify notations, let us define $q := \text{dz}(u_{\text{FB}})$ and $\zeta := [\varepsilon\ x_c]^\top$, so that dynamics (12) can be expressed in the compact form

$$\dot{\zeta} = \underbrace{\begin{bmatrix} -1/\tau & 0 \\ 1 & 0 \end{bmatrix}}_{A}\zeta - \underbrace{\begin{bmatrix} 1/\tau \\ 0 \end{bmatrix}}_{B}\underbrace{[k_P\ k_I]}_{K}\zeta + \underbrace{\begin{bmatrix} 1/\tau \\ 0 \end{bmatrix}}_{B_q} q + \underbrace{\begin{bmatrix} 0 \\ 1 \end{bmatrix}}_{B_{aw}} k_{aw} q. \tag{13}$$

3.2 LMI-based design

Now, we want to build an LMI formulation that can consider all the constraints in order to design the gains (k_I, k_P, k_{aw}) of the controller. The main objective is to ensure the stability of the closed-loop dynamics (13) with a given decay rate $\alpha > 0$. To this end, let us consider the nonnegative quadratic Lyapunov function $V(\zeta) = \zeta^\top P\zeta$, with $P = P^\top \succ 0$. Then, the stability and the decay rate are ensured if

$$\dot{V}(\zeta) = 2\zeta^\top P\dot{\zeta} < -2\alpha V(\zeta). \tag{14}$$

Since q is the deadzone nonlinearities, the scalar sector condition $qw(u_{\text{FB}} - q) \geq 0$ holds for every $w > 0$. Therefore, following the procedure in (Zaccarian and Teel, 2011, Sec 3.4.3), in order to guarantee the previous conditions, it is enough to check

$$2\zeta^\top P\dot{\zeta} + 2qw(u_{\text{FB}} - q) + 2\alpha V(\zeta) < 0,$$

where $u_{\text{FB}} = K\zeta$. This expression can be developed in an equivalent matrix form

$$2\begin{bmatrix} z \\ q \end{bmatrix}^\top \underbrace{\begin{bmatrix} P(A - BK + \alpha I) & P(B_q + B_{aw}k_{aw}) \\ wK & -w \end{bmatrix}}_{M} \begin{bmatrix} z \\ q \end{bmatrix} < 0, \tag{15}$$

which is equivalent to the bilinear matrix inequality $\text{He}(M) \prec 0$ in the unknowns $P \in \mathbb{S}^2$, $K \in \mathbb{R}^{1\times 2}$, $k_{aw} > 0$, and $w > 0$. Then, by multiplying it left and right by

$$\begin{bmatrix} S & 0 \\ 0 & v \end{bmatrix} = \begin{bmatrix} P^{-1} & 0 \\ 0 & w^{-1} \end{bmatrix},$$

and applying a change of variable, we obtain

$$\text{He}\left(\begin{bmatrix} (A + \alpha I)S - BY & B_q v + B_{aw} r \\ Y & -v \end{bmatrix}\right) \prec 0, \tag{16}$$

which is an LMI in the unknowns $S \in \mathbb{S}^n$, $Y := KS \in \mathbb{R}^{1\times 2}$, $v > 0$, and $r := vk_{aw} > 0$. Therefore, if LMI (16) is feasible the linearized closed-loop system is stable.

To make our design robust, we consider that the parameter Q, related to the load R, can vary in a range $[Q_{min}, Q_{max}]$. The uncertainty extends to the time constant of the identified first-order system (10) since $\tau = \frac{2Q}{\omega_0}$. This can be easily taken into account by imposing LMI (16) twice, with the matrices A, B, and B_q evaluated at τ_{min} and τ_{max}. Then, the gains can be found by solving the following optimization problem with an LMI solver for a fixed decay rate α:

$$\begin{aligned} \min_{S,Y,v,r}\ & v, \quad \text{subject to:} \\ & S \succ 0, \quad v > 0, \\ & \text{He}\left(\begin{bmatrix} (A_i + \alpha I)S - B_i Y & B_{q_i} v + B_{aw} r \\ Y & -v \end{bmatrix}\right) \prec 0, \\ & \text{for all } i = 1, 2, \end{aligned} \tag{17}$$

where A_i, B_i and B_{q_i} are the matrices on the vertices of the polytope defined by the uncertainty. Controller gains are then derived by

$$K = YS^{-1} \quad \text{and} \quad k_{aw} = r/v. \tag{18}$$

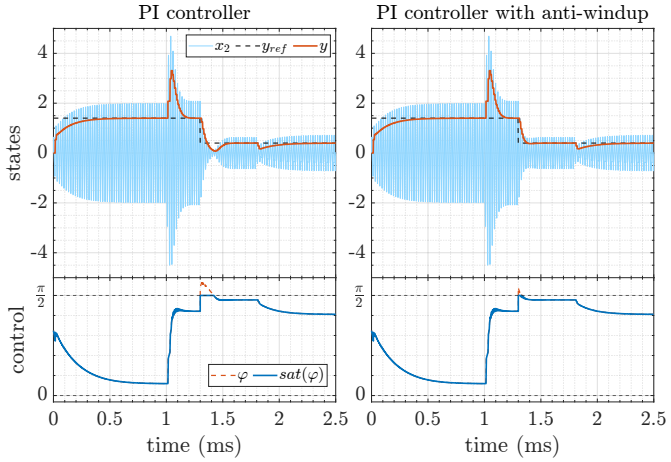

Fig. 6. Simulation without (left) and with (right) anti-windup. Top: state x_2 (dotted-blue), reference y_{ref} (dashed-black), and RMS value y (orange). Bottom: computed φ (dashed-orange) and saturated φ (blue). Perturbations on the load are at 1 ms and 1.8 ms.

4. SIMULATION

To validate the proposed control scheme, simulations are performed in MATLAB/Simulink, with a PLECS module for the circuit, and a simulation step of 5 ns. Circuit parameters and corresponding system characteristics are given in Table 1.

Optimization problem (17) is solved using MATLAB and the SDP solver MOSEK 10.1, the parameters are $\alpha = 15500$ and $Q \in [1, 10]$. The resulting controller gains are:

$$k_P = 1.13, \qquad k_I = 3.30 \times 10^4, \qquad k_{aw} = -22.69.$$

To analyze the performances of the controller, the RMS value reference y_{ref} and the load R change during the simulation. Simulation starts with $y_{ref} = 1.4$. The reference is changed to 0.4 at $t = 1.3$ ms. Similarly, simulation starts with $R = 2\,\Omega$, which is equivalent to $Q = \frac{1}{R}\sqrt{\frac{L}{C}} = 1.58$; then the load is affected by a step perturbation at $t = 1$ ms becoming $R = 0.5\,\Omega$, which is equivalent to $Q = 6.32$; finally, the load is set back to $R = 2\,\Omega$ at $t = 1.8$ ms.

Fig. 6 shows simulation results with and without the anti-windup loop to highlight its contribution to the system behavior. In both cases, the estimated RMS output y converges to the reference after a short transient time.

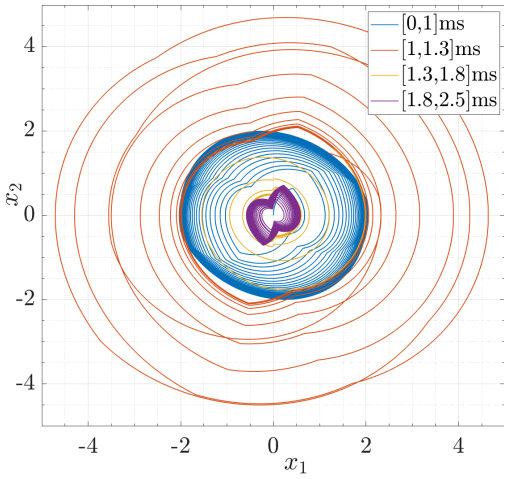

Fig. 7. Phase portrait of the system with anti-windup.

After the change of reference, φ saturates at $\frac{\pi}{2}$; during this phase, the anti-windup loop allows to limit the saturation time and the induced output overshoot. Even with the lowest Q value, the output stabilizes to the desired reference, showing the efficiency of the proposed control scheme and associated gains tuning process.

Fig. 7 pictured the phase plane of the closed-loop system, with different colors to distinguish changes of parameters during the simulation. When perturbations appear, the system stabilizes to a new limit cycle while keeping the same desired RMS value; as expected, the shape of the limit cycle is different and it depends on Q. Notice that the limit cycle is not always close to a circle shape, meaning that the outer controller is able to compensate when signals are not completely sinusoidal.

5. FINAL DISCUSSION

This work proposed a simple controller scheme for the RMS value regulation thanks to a first-harmonic analysis. A hybrid dynamical system is used to estimate the RMS value of the output current. Futures works may aim at exploring this kind of scheme for constant power control, also an experimental implementation could be foreseen.

ACKNOWLEDGEMENTS

We want to thank our colleagues of the MAC team that gave use advice, their support, and encouraged us to pursue this work.

REFERENCES

Bonache-Samaniego, R., Olalla, C., and Martínez-Salamero, L. (2017). Dynamic Modeling and Control of Self-Oscillating Parallel Resonant Converters Based on a Variable Structure Systems Approach. *IEEE Transactions on Power Electronics*, 32(2), 1469–1480.

Cavalcante, F. (2006). *High Output Voltage Series-Parallel Resonant DC-DC Converter for Medical X-ray Imaging Applications*. Ph.D. thesis, Swiss Federal Institute of technology Zurich.

Deng, J., Li, S., Hu, S., Mi, C.C., and Ma, R. (2014). Design Methodology of LLC Resonant Converters for Electric Vehicle Battery Chargers. *IEEE Transactions on Vehicular Technology*, 63(4), 1581–1592.

Erickson, R.W. and Maksimović, D. (2020). *Fundamentals of Power Electronics*. Springer International Publishing.

Goebel, R., Sanfelice, R., and Teel, A. (2012). *Hybrid Dynamical Systems: Modeling, Stability, and Robustness*. Princeton University Press.

Lucia, O., Burdio, J.M., Millan, I., Acero, J., and Puyal, D. (2009). Load-Adaptive Control Algorithm of Half-Bridge Series Resonant Inverter for Domestic Induction Heating. *IEEE Transactions on Industrial Electronics*, 56(8), 3106–3116.

Mohammadi, M. and Ordonez, M. (2016). Fast transient response of series resonant converters using average geometric control. *IEEE Transactions on Power Electronics*, 31(9), 6738–6755.

Oruganti, R., Yang, J.J., and Lee, F.C. (1987). Implementation of optimal trajectory control of series resonant converter. In *1987 IEEE Power Electronics Specialists Conference*, 451–459.

Pinheiro, H., Jain, P., and Joos, G. (1999). Self-sustained oscillating resonant converters operating above the resonant frequency. *IEEE Transactions on Power Electronics*, 14(5), 803–815.

Pitel, I.J. (1986). Phase-Modulated Resonant Power Conversion Techniques for High-Frequency Link Inverters. *IEEE Transactions on Industry Applications*, IA-22(6), 1044–1051.

Sebastián, E., Montijano, E., Oyarbide, E., Bernal, C., and Gálvez, R. (2022). Nonlinear implementable control of a dual active bridge series resonant converter. *IEEE Transactions on Industrial Electronics*, 69(5), 5111–5121.

Tarbouriech, S., Garcia, G., Gomes Da Silva, J.M., and Queinnec, I. (2011). *Stability and Stabilization of Linear Systems with Saturating Actuators*. Springer, London.

Yin, Y., Zane, R., Glaser, J., and Erickson, R. (2003). Small-signal analysis of frequency-controlled electronic ballasts. *IEEE Transactions on Circuits and Systems I: Fundamental Theory and Applications*, 50(8), 1103–1110.

Youssef, M. and Jain, P. (2004). A review and performance evaluation of control techniques in resonant converters. In *30th Annual Conference of IEEE Industrial Electronics Society, 2004.*, volume 1, 215–221 Vol. 1.

Zaccarian, L. and Teel, A.R. (2011). *Modern Anti-windup Synthesis: Control Augmentation for Actuator Saturation*. Princeton University Press.

Zaupa, N., Olalla, C., Queinnec, I., Martínez-Salamero, L., and Zaccarian, L. (2023). Hybrid Control of Self-Oscillating Resonant Converters With Three-Level Input. *IEEE Control Systems Letters*, 7, 1375–1380.